Spin-chiral domains in $Ba_{0.5}Sr_{1.5}Zn_2Fe_{12}O_{22}$ observed by scanning resonant x-ray microdiffraction

Y. Hiraoka,[1] Y. Tanaka,[2] T. Kojima,[2,3] Y. Takata,[2,3] M. Oura,[2] Y. Senba,[4] H. Ohashi,[4] Y. Wakabayashi,[1] S. Shin,[2] and T. Kimura[1,*]

[1]*Division of Materials Physics, Graduate School of Engineering Science, Osaka University, Toyonaka, Osaka 560-8531, Japan*

[2]*RIKEN SPring-8 Center, Sayo, Hyogo 679-5148, Japan*

[3]*Department of Complexity Science and Engineering, University of Tokyo, Kashiwa, Chiba 277-8561, Japan*

[4]*Japan Synchrotron Radiation Research Institute (JASRI), Sayo, Hyogo 679-5198, Japan*

(Received 28 April 2011; revised manuscript received 1 July 2011; published 22 August 2011)

In magnetic materials showing helimagnetic orders, "spin chirality" is one of the key order parameters to describe their electronic properties and often induces unique physical phenomena related to its symmetry breakings. Thus, observation of its domain structure, that is, the spin-chiral domain structure, is essential to fully understand the properties of helimagnetic materials. However, such domain structures are largely uninvestigated because of a lack of technique. Here, we report spatial maps of spin-chiral domains in helimagnetic $Ba_{0.5}Sr_{1.5}Zn_2Fe_{12}O_{22}$ by means of a scanning resonant x-ray microdiffraction technique using circularly polarized x rays. The use of a highly focused incident x-ray beam allows the observation of self-organizing spin-chiral domain patterns with the highest contrast ever achieved in helimagnetic materials. Our results demonstrate that the technique provides a powerful tool to investigate the spin-chiral domain structure.

DOI: 10.1103/PhysRevB.84.064418 PACS number(s): 61.05.cp, 75.25.−j, 75.60.−d

I. INTRODUCTION

Helimagnetic orders have been studied in various magnetic materials since they were first proposed by Yoshimori in 1959[1] and have recently been attracting renewed interest because of their unique influences on dielectric and transport properties (e.g., spin-driven ferroelectricity[2] and anomalous magnetotransport[3]). In such electronic properties, spin chirality, i.e., right- or left-handedness of an ordered magnetic state, plays an important role. In magnetic noncentrosymmetric crystals, spin chirality is determined by the sign of the antisymmetric Dyaloshinskii-Moriya interaction.[4–6] Meanwhile, in centrosymmetric crystals possessing spin chirality that arises because of geometric frustration, right- and left-handed chiral states are energetically equivalent in the absence of applied fields.[7] This should give rise to a spin-chiral domain structure like the magnetic (ferroelectric) domains observed in ferromagnets (ferroelectrics). However, observation of the spin-chiral domain structure is not as straightforward as that of the preceding ferroic domains. To date, the spin-chiral domains have been observed mainly for rare earth metals (e.g., Tb and Ho) by only a few experimental techniques, such as diffraction topography using polarized neutrons[8,9] and scanning x-ray microdiffraction using circularly polarized x rays.[10,11] The scanning x-ray microdiffraction has often been applied to observe spin-chiral-domain structure and its population in a class of multiferroics in which chiral magnetic structures induce ferroelectricity.[12,13] In these previous studies, however, the probe size, i.e., the cross-section area of x-ray beam, is on an order of submillimeter ($\approx 300 \times 100\ \mu m^2$ for Ref. 12 and $\approx 380 \times 250\ \mu m^2$ for Ref. 13), which has prevented observation of the essential features of naturally formed spin-chiral domains.

In this paper, we report the observation of spin-chiral domains on a clean cleaved surface of a helimagnetic hexaferrite, $Ba_{0.5}Sr_{1.5}Zn_2Fe_{12}O_{22}$, by means of the scanning x-ray microdiffraction technique using a circularly polarized and highly focused x-ray beam with its cross section $\approx 30 \times 15\ \mu m^2$. By tuning the x-ray photon energy to the Fe L_3 edge, where a $2p$ core electron is excited into an empty and magnetically aligned $3d$ state, an increase in the sensitivity for the spin state of the valence electron can be achieved. Our experimental setting provides the necessary resolution and contrast to resolve self-organized spin-chiral domains with a submillimeter-length scale on clean surfaces of the helimagnetic hexaferrite.

The hexaferrite $Ba_{0.5}Sr_{1.5}Zn_2Fe_{12}O_{22}$ was recently found to show magnetic-field-induced ferroelectricity triggered by a metamagnetic transition.[14] Its crystal structure with the centrosymmetric space group $R\bar{3}m$ ($a \approx 5.86$ Å and $c \approx 43.4$ Å in the hexagonal setting) is composed of alternating stacks of S and L blocks along the c axis [Fig. 1(a)]. In $Ba_{0.5}Sr_{1.5}Zn_2Fe_{12}O_{22}$, a helical spin ordered state with two chiral domains, illustrated in Figs. 1(b) and 1(c), is stabilized below $T_N \approx 320$ K, which originates from the competing magnetic interactions across the boundary of the L and S blocks.[15] The helimagnetic structure results in the appearance of magnetic satellite peaks on both sides of Bragg reflections at $(0\ 0\ 3n \pm \varepsilon)$ with $n =$ integer, which has been studied by neutron and resonant x-ray diffraction techniques.[15,16] The turn angle of the helix φ given by $\varphi = 2\pi\varepsilon/3$ is 180° just below T_N, decreases with decreasing temperature, and becomes a nearly constant value (∼84°) below ∼100 K.

II. EXPERIMENTAL DETAILS

Single crystals of $Ba_{0.5}Sr_{1.5}Zn_2Fe_{12}O_{22}$ were grown by a flux method using Na_2O-Fe_2O_3 flux, as reported previously.[17] The starting composition as a mole percentage was 2.95 $BaCO_3$, 16.74 $SrCO_3$, 19.69 ZnO, 53.61 Fe_2O_3, and 7.01 Na_2CO_3. The mixture was packed into a platinum crucible, heated at 1420 °C in a furnace for 20 hours, and then slowly cooled to 1100 °C in air. To remove a by-product phase ($ZnFe_2O_4$), the temperature cycling method was used.

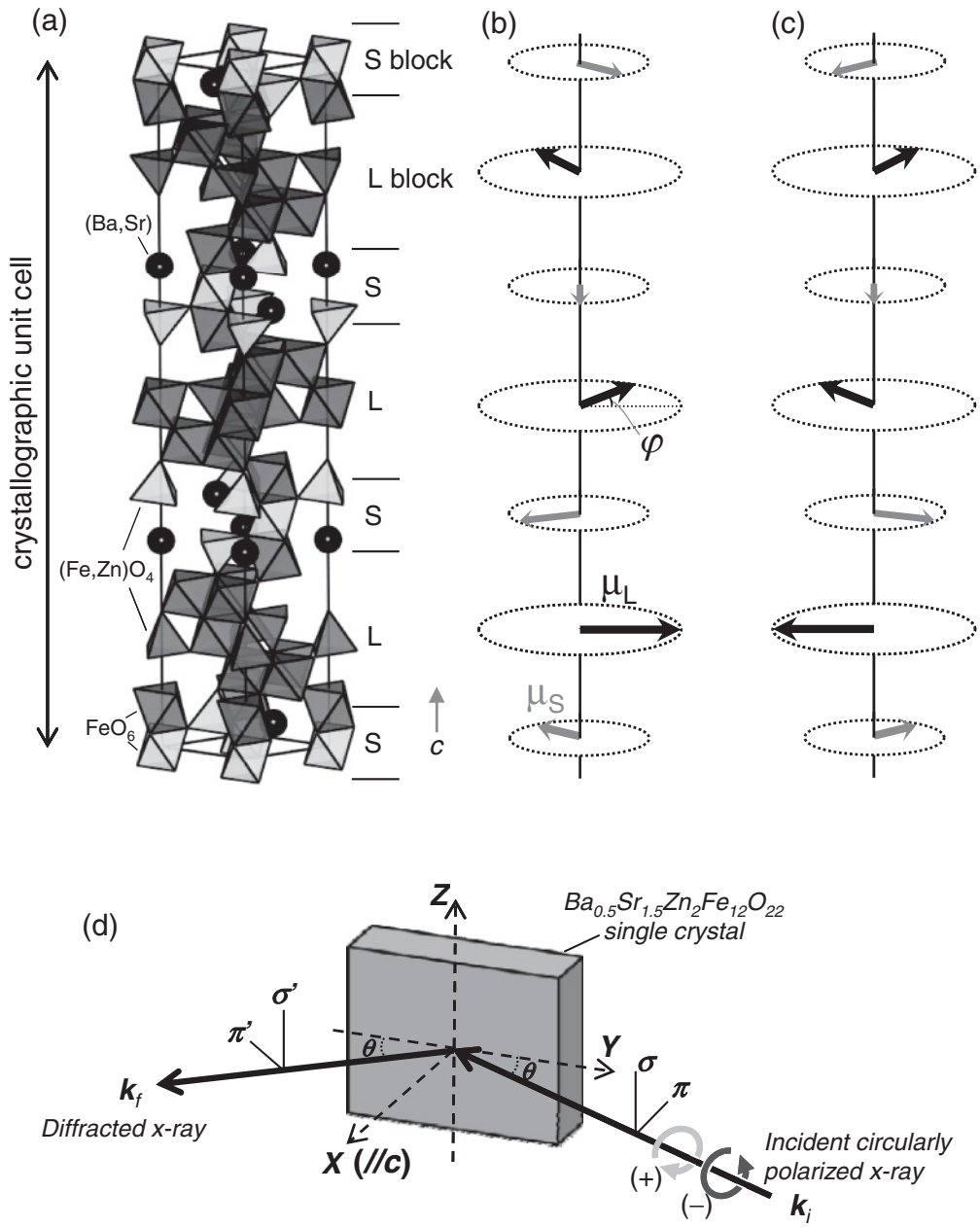

FIG. 1. Crystallographic and helimagnetic structures of $Ba_{0.5}Sr_{1.5}Zn_2Fe_{12}O_{22}$. (a) Crystal structure composed of alternating stacks of S and L blocks. (b) and (c) Right- and left-handed spin-chiral structures, respectively. (d) Schematic illustration of the scattering geometry. Here, $\boldsymbol{k}_i$ and $\boldsymbol{k}_f$ are the propagation vectors of the incident and diffracted x rays, respectively, and θ denotes the Bragg angle. The σ and σ' components are perpendicular to the scattering plane, and the π and π' components are parallel to the scattering plane.

After cooling to room temperature, the crystals were leached from the crucible with hot, diluted nitric acid. The obtained crystals had a typical dimension of $\sim 5 \times 5 \times 2$ mm^3. The temperature dependence of the magnetization was measured for the crystals in a magnetic field of 5 mT along the c axis and showed a sharp peak $\sim$310 K. This suggests that an antiferromagnetic ordering takes place $\sim$310 K. For measurements of resonant x-ray magnetic diffraction, these crystals were cleaved at an ambient condition, and clean and flat surfaces normal to the c axis (surface dimensions $\sim 5 \times 4$ mm) were obtained.

Measurements of resonant x-ray magnetic diffraction of the cleaved surfaces were carried out using an ultra-high-vacuum diffractometer equipped at the beamline 17SU, SPring-8, Japan.[18] The incident photon energy was tuned to the Fe L_3 edge (=710 eV). The helicity of the incident beam was switched by electromagnets of an undulator. The polarization of x rays is defined by two orthogonal unit vectors $\boldsymbol{e}^{(1)}$ and $\boldsymbol{e}^{(2)}$ represented by σ and π, respectively, as illustrated in Fig. 1(d). The scattering plane is spanned by vectors $\boldsymbol{k}_i$ and $\boldsymbol{k}_f$, which are the propagation vectors of the incident and diffracted beams, respectively. Vectors $\boldsymbol{k}$, $\boldsymbol{e}^{(1)}$, and $\boldsymbol{e}^{(2)}$ have the right-handed

relation $\frac{\boldsymbol{k}}{|\boldsymbol{k}|} = \boldsymbol{e}^{(1)} \times \boldsymbol{e}^{(2)}$. Here, we denote the vectors of the right- and left-handed circular polarization by $\boldsymbol{e}^{(+)}$ and $\boldsymbol{e}^{(-)}$, respectively, and define the helicity as positive and negative, respectively, as well:[19]

$$\boldsymbol{e}^{(\pm)} = \mp\frac{i}{\sqrt{2}}(\boldsymbol{e}^{(1)} \pm i\boldsymbol{e}^{(2)}). \quad (1)$$

The circular polarization is expressed by a sum of $\boldsymbol{e}^{(1)}$ and $\boldsymbol{e}^{(2)}$ linear polarization, and the + (−) helicity beam that has the $\boldsymbol{e}^{(1)}$ component is advanced (behind) in time by a phase $\frac{\pi}{2}$ to the $\boldsymbol{e}^{(2)}$ component at the fixed position with the expression of the phase factor $\exp i\,(\boldsymbol{k}\cdot\boldsymbol{r} - \omega t)$ for an electromagnetic plane wave. In other words, when the observer is looking toward the beam source, the electric field of the + (−) helicity beam is counterclockwise (clockwise) in time [Fig. 1(d)] and has a left- (right-)handed screw-in space. Many textbooks for crystallography conventionally use the opposite sign for the phase factor, whereas our definition of handedness is opposite to that of optics.

The crystals were mounted with the c axis in the scattering plane, as illustrated in Fig. 1(d). The penetration depth ξ of the incident beam into the hexaferrite crystal was estimated from the full width at half maximum ΔQ of the (0 0 3) Bragg reflection. By using the relation, $\xi = 2\pi/\Delta Q$, where the unit of ΔQ is the reciprocal nanometer, we obtained $\xi \approx 40$ nm at the Fe L_3 edge. For the imaging, the crystal was positioned with an XYZ translation stage with a 25-μm step, and the diffracted intensity of the (0 0 3–ε) magnetic reflection was measured at each point using a Si-photodiode sensor. (As depicted in Fig. 1(d), the X direction is aligned along the c axis and in the Z direction is perpendicular to the scattering plane.) We focused the incident beam using Kirkpatrick-Baez configuration mirrors equipped just before the diffractometer.[20] The spot size was ∼30 μm in horizontal and 15 μm in vertical directions, which gives spatial resolutions for Y and Z scans of ∼60 and 15 μm, respectively.

III. RESULTS AND DISCUSSION

Figure 2(a) shows (0 0 L) scans between the (0 0 2) and the (0 0 4) positions at 74 K on a certain sample position ($Y = 0.5$, $Z = 0$). Along with the (0 0 3) Bragg reflection, two magnetic satellite peaks are evident at (0 0 $3 \pm \varepsilon$) with $\varepsilon = 0.64$. The sign change in the helicity of the circularly polarized incident x rays yields substantially different intensities of the magnetic reflections. The (0 0 $3 - \varepsilon$) reflection is more intense for incident x rays with the positive (+) helicity than with the negative (−) one, whereas (0 0 $3 + \varepsilon$) by (+) helicity x rays is weaker than that by (−) ones. This result is essentially consistent with a previous resonant x-ray diffraction study.[16] However, the helicity-dependent magnitude relations of the (0 0 $3 \pm \varepsilon$) intensities were reversed completely at another sample position ($Y = 1.1$, $Z = 0$), as displayed in Fig. 2(b). For the data shown in Fig. 2(a), the ratios of the (0 0 $3 \pm \varepsilon$) intensities obtained by (−) helicity x rays to those by (+) ones are $I_{(003-\varepsilon)}{}^{(-)}/I_{(003-\varepsilon)}{}^{(+)} = 0.24$ and $I_{(003+\varepsilon)}{}^{(-)}/I_{(003+\varepsilon)}{}^{(+)} = 5.8$. Meanwhile, $I_{(003-\varepsilon)}{}^{(-)}/I_{(003-\varepsilon)}{}^{(+)} = 4.8$ and $I_{(003+\varepsilon)}{}^{(-)}/I_{(003+\varepsilon)}{}^{(+)} = 0.20$ for the data of Fig. 2(b). These results suggest that the spin chirality in these two positions are opposite in sign to each other.

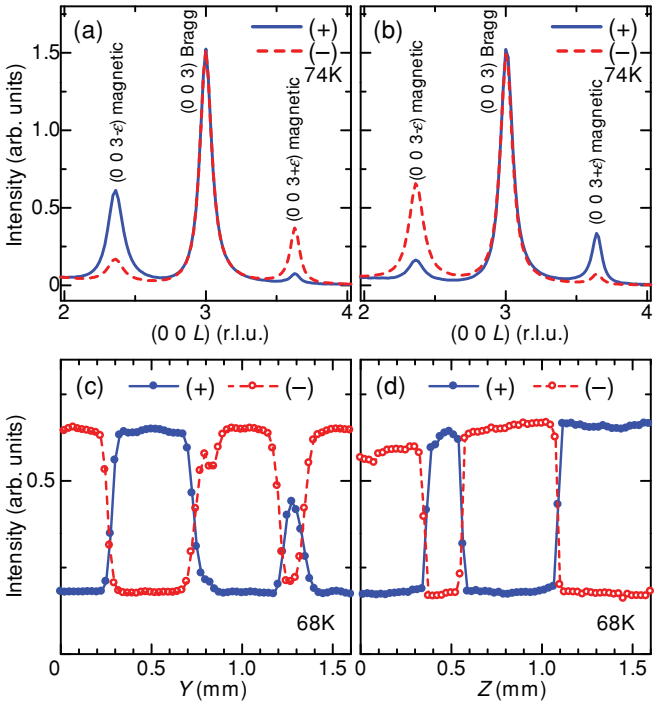

FIG. 2. (Color online) Sample position and circular x-ray polarization dependence of magnetic reflection intensity. (a) and (b) X-ray diffraction profiles of the (0 0 L) scan measured at different sample positions 0.6 mm distant. (c) and (d) X-ray peak intensities of the (0 0 3–ε) reflection as functions of horizontal (Y) and vertical (Z) sample positions, respectively. These measurements were carried out using (−) (broken red lines) and (+) (solid blue lines) helical incident x rays with an energy corresponding the Fe L_3 edge.

The resonant intensity of the magnetic satellites for the helimagnetic structure of the hexaferrite has been formulated by Mulders *et al.*[16] According to their calculation, the magnetic diffraction intensity along the c axis from right- and

TABLE I. The observed intensity ratios of $I_{(003\pm\varepsilon)}{}^{(-)}$ to $I_{(003\pm\varepsilon)}{}^{(+)}$, and the calculated fraction of the right-handed spin-chiral domains for the data shown in Figs. 2(a) and 2(b).

	Fig. 2(a) (at $Y = 0.5$, $Z = 0$)		Fig. 2(b) (at $Y = 1.1$, $Z = 0$)	
magnetic reflection	(0 0 $3 - \varepsilon$)	(0 0 $3 + \varepsilon$)	(0 0 $3 - \varepsilon$)	(0 0 $3 + \varepsilon$)
θ (degree)	28.4	47.0	28.4	47.0
$I^{(-)}/\,I^{(+)}$	0.24	5.8	4.8	0.20
a (fraction of right-handed domain)	97.2%	100%	0.2%	2.8%

left-handed spin-chiral domains for circularly polarized x rays are given by

$$I_{\text{right}} \propto \left(\cos^2\theta + \tfrac{1}{2}\sin^2 2\theta \mp \chi \cos\theta \sin 2\theta\right) \times [F_{11} - F_{1-1}]^2 \delta(\boldsymbol{q} - 3n\boldsymbol{G} \pm \varepsilon), \quad (2)$$

$$I_{\text{left}} \propto \left(\cos^2\theta + \tfrac{1}{2}\sin^2 2\theta \pm \chi \cos\theta \sin 2\theta\right) \times [F_{11} - F_{1-1}]^2 \delta(\boldsymbol{q} - 3n\boldsymbol{G} \pm \varepsilon). \quad (3)$$

where F_{11} and F_{1-1} are the atomic properties of the initial and excited states of the Fe ion, and $\boldsymbol{q}$ $(=\boldsymbol{k}_i - \boldsymbol{k}_f)$, $\boldsymbol{G}$, $\boldsymbol{\varepsilon}$, and θ denote the wave vector transfer between incident and diffracted radiation, the reciprocal lattice vector, the magnetic propagation vector, and the Bragg angle, respectively. $\chi = +1$ for the (+) helicity of the incident beam, whereas $\chi = -1$ for the (−) helicity. If the fractions of the right- and left-handed spin-chiral domains on the area irradiated by the x-ray beam are a and $(1 - a)$, respectively, the diffracted intensity is given by

$$I_a \propto \left(\cos^2\theta + \tfrac{1}{2}\sin^2 2\theta \pm (1-2a)\chi \cos\theta \sin 2\theta\right) \times [F_{11} - F_{1-1}]^2 \delta(\boldsymbol{q} - 3n\boldsymbol{G} \pm \boldsymbol{\varepsilon}). \quad (4)$$

Thus, the intensity ratio by the incident x-ray beam with the (−) helicity to that with the (+) helicity for the $(0\ 0\ 3n \pm \varepsilon)$ magnetic reflection can be written as

$$I_a^{(-)}/I_a^{(+)} = \frac{\cos^2\theta + \frac{1}{2}\sin^2 2\theta \mp (1-2a)\cos\theta \sin 2\theta}{\cos^2\theta + \frac{1}{2}\sin^2 2\theta \pm (1-2a)\cos\theta \sin 2\theta}. \quad (5)$$

By applying Eq. (5) to the present experimental data, the population ratio between the right- and the left-handed spin chiral domains at a beam spot can be estimated. The results are summarized in Table I and demonstrate that the area measured for the data shown in Figs. 2(a) and 2(b) consists of nearly a monodomain with the right- and left-handed spin-chiral states, respectively. These results also confirm that

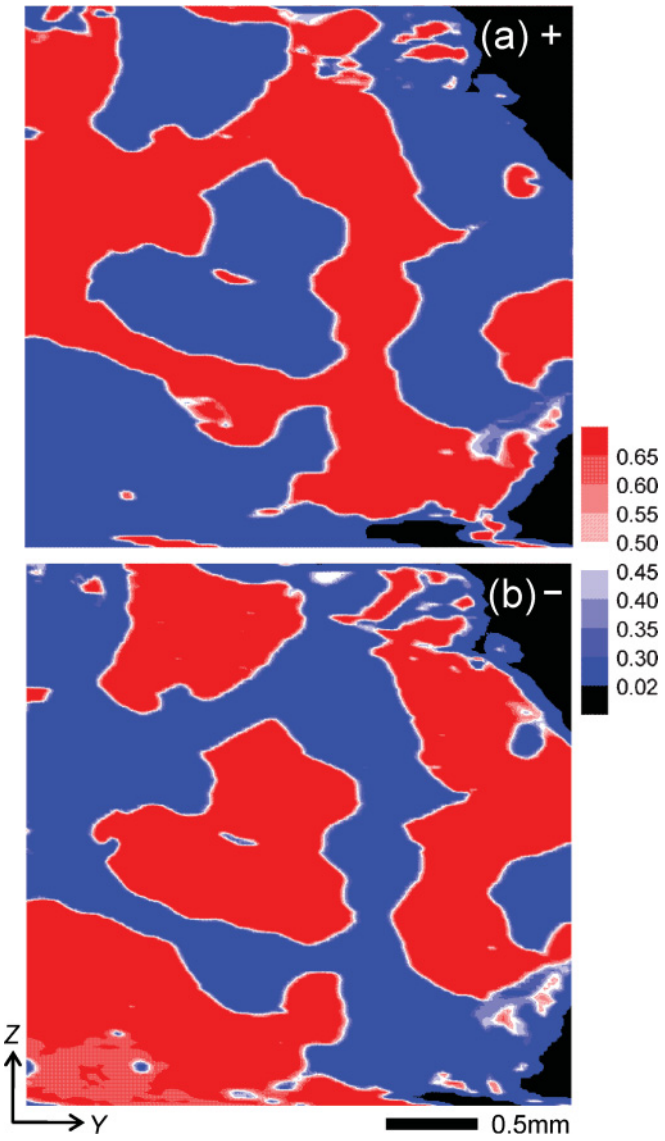

FIG. 3. (Color online) Spatial images of the spin-chiral domain structure in a single crystal of $Ba_{0.5}Sr_{1.5}Zn_2Fe_{12}O_{22}$. (a) and (b) X-ray intensity maps of the $(0\ 0\ 3-\varepsilon)$ magnetic reflection measured over a 3×3 mm^2 area at 68 K using (+) and (−) helical incident x rays, respectively. Red (bright) and blue (dark) regions correspond to either a left- or right-handed spin-chiral domain. Black-coloured areas represent off-sample regions.

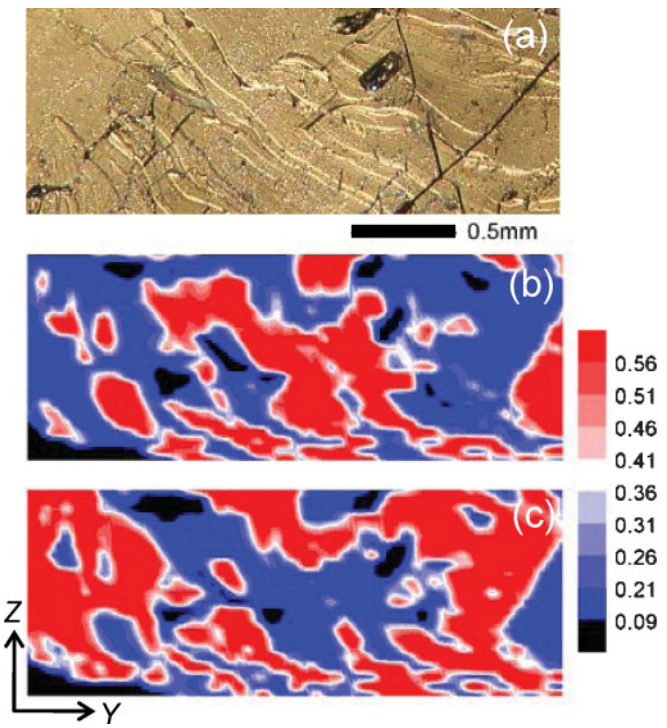

FIG. 4. (Color online) Spatial images of the spin-chiral domain structure in a crystal of $Ba_{0.5}Sr_{1.5}Zn_2Fe_{12}O_{22}$ with a rough surface. (a) Photograph of the scanned surface of the crystal. (b) and (c) X-ray intensity maps of the $(0\ 0\ 3-\varepsilon)$ magnetic reflection measured at 75 K using (−) and (+) helical incident x rays, respectively. Red (bright) and blue (dark) regions correspond to either a left- or right-handed spin-chiral domain. Black areas represent regions with low intensities because of the roughness of the surface.

the spatial resolution is small enough to isolate "a single chiral domain."

To further verify the sample position dependence of the spin chirality, we performed a microdiffraction scan in the Y and Z directions at the (0 0 3−ε) position with both (+) and (−) helical incident x rays. Figures 2(c) and 2(d) displays the intensity profiles of the (0 0 3−ε) magnetic reflection as functions of the Y and Z positions, respectively, at 68 K. Two discrete levels of the intensity alternately appear with a step width of 0.1 ∼ 0.6 mm. More importantly, the intensity at each position is switched by changing the sign of the incident x-ray helicity, which means that the intensity profiles shown in Figs. 2(c) and 2(d) correspond to cross sections of spin-chiral domains. Thus, the present experimental setup of scanning resonant x-ray microdiffraction allows spin-chiral domains to be mapped by setting the sample to diffract on the magnetic satellite and scanning it through the x-ray beam.

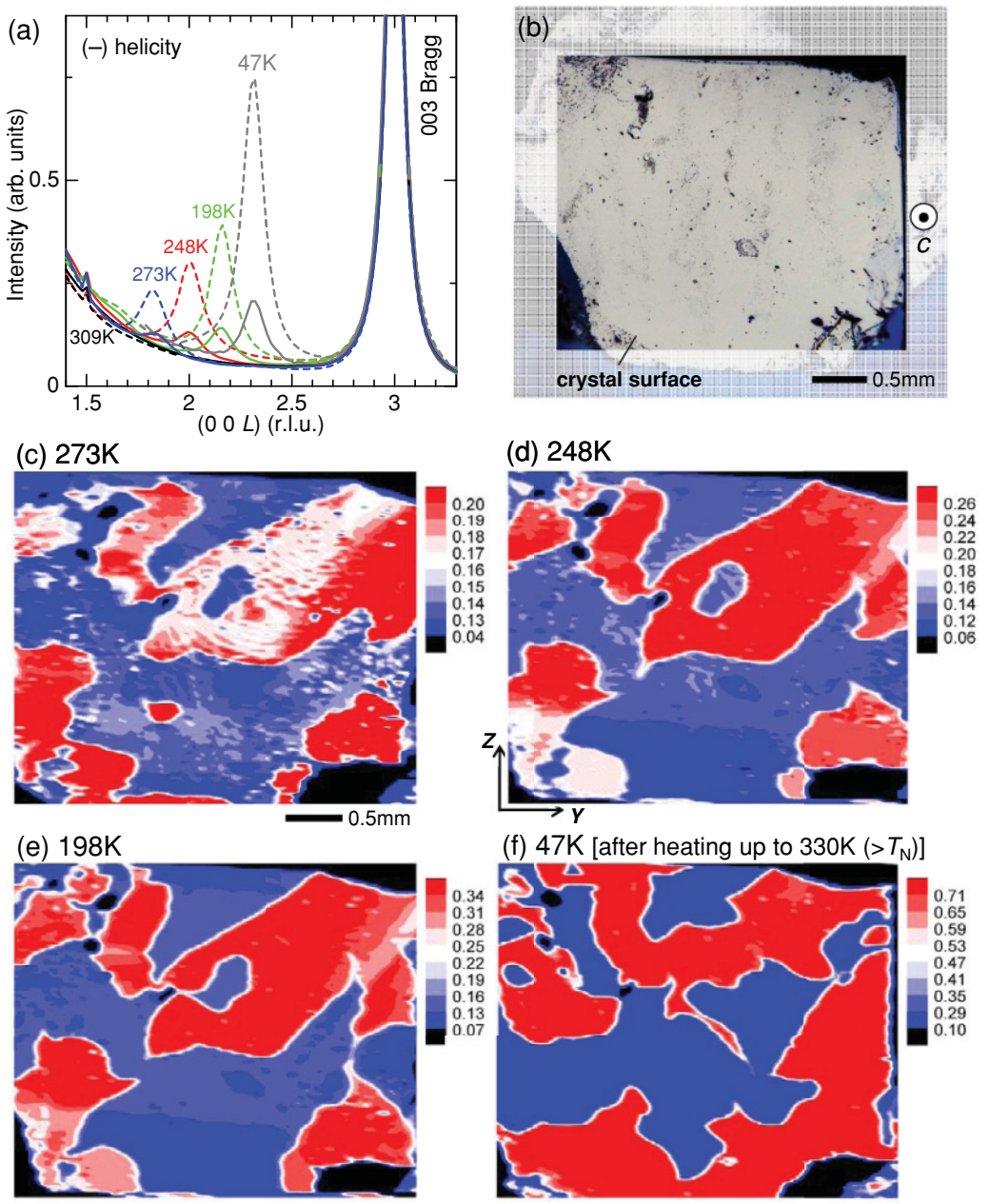

FIG. 5. (Color online) Temperature evolution of the spin-chiral domain structure in a single crystal of $Ba_{0.5}Sr_{1.5}Zn_2Fe_{12}O_{22}$. (a) X-ray diffraction L scans along (0 0 L) at various temperatures. A small peak at $L = 1.5$ corresponds to the second harmonic of the (0 0 3) Bragg reflection. Broken and solid lines represent the reflections from a left- and a right-handed spin-chiral domain, respectively. (b) Photograph of the scanned surface of the crystal. (c)–(f) Spatial images of the spin-chiral domain structure at selected temperatures. These measurements were done using (−) helical incident x rays at 273 K (c), 248 K (d), 198 K (e), and 47 K (f). Before the measurement at 47 K (f), the sample was heated to 330 K ($>T_N$).

Figure 3 shows a two-dimensional *YZ*-scanned intensity map of the (0 0 3−ε) magnetic reflection, i.e., a spin-chiral domain structure, over a 3 × 3 mm^2 area at 68 K. Bright (red) and dark (blue) correspond to high- and low-intensity counts, respectively. The images shown in Figs. 3(a) and 3(b) were taken at the same sample area by using (+) and (−) helical incident x rays, respectively. The color contrast is quite high and reversed from the image of Fig. 3(a) to that of Fig. 3(b). This confirms that the bright (red) and dark (blue) regions in the image of Fig. 3(b) correspond to a left- and a right-handed spin-chiral monodomain, respectively, which covers almost all regions. The observed domains are irregular in shape, with a size on a submillimeter scale. The left- and right-handed spin-chiral domains are nearly equally populated. White boundaries, which are quite thin, correspond to the domain walls, which have no simple crystallographic orientations. By comparing the cross sections along the *Y* and *Z* axes shown in Figs. 2(c) and 2(d), we see that domain boundaries for the *Z* scan data are narrower than those for the *Y* scan data. This is because of better spatial resolution along the *Z* axis. The thickness is unknown with our resolution, but it is at least <50 μm, which is estimated by a deconvolution with the beam size. To our knowledge, the images shown in Fig. 3 have the highest contrast ever achieved for the magnetic chiral domains.

Compared with spin-chiral domains observed in helimagnetic rare earth metals, the domain pattern (curved wall shape) and size (submillimeter scale) in the hexaferrite are somewhat similar to those in high-purity Tb and Ho single crystals after cooling from a paramagnetic phase.[8,9] In the rare earth metals, the size of spin-chiral domains was found to be sensitive to the crystal purity (e.g., less than ∼0.06 mm in an impure sample).[8,9] We also performed scanning resonant x-ray microdiffraction measurements of another crystal of $Ba_{0.5}Sr_{1.5}Zn_2Fe_{12}O_{22}$ with a rougher surface. Figure 4(a) displays a photograph of the surface. As seen in Fig. 4(a), the measured surface contains some defects such as dents, cracks, and steps. Figures 4(b) and 4(b) shows two-dimensional intensity maps of the (0 0 3−ε) magnetic reflection at 75 K. Bright (red) and dark (blue) correspond to high- and low-intensity counts, respectively. The images shown in Figs. 4(b) and 4(c) were taken at the same sample area by using (−) and (+) helical incident x rays, respectively. The color contrast is reversed from the image of Fig. 4(b) to that of Fig. 4(c), which confirms that bright (red) and dark (blue) regions correspond to either a left- or a right-handed spin-chiral domain. By closely comparing the surface photograph shown in Fig. 4(a) and the domain structure shown in Figs. 4(b) and 4(c), we find a tendency for the domain boundaries to be clamped at surface defects such as cracks, steps, and dents. In addition, the observed domains in the crystal were apparently smaller than those on a smooth surface (cf. Fig. 4 with Fig. 3). The result appears to be similar to the case of the helimagnetic rare earth metals.

To examine the evolution of the domain structure as a function of temperature, we measured two-dimensional intensity maps of the (0 0 3−ε) magnetic reflection at several temperatures for the crystal used in the measurements of Fig. 3. All measurements shown here were done using incident x rays with (−) helicity. Before every mapping measurement, we checked the position of the (0 0 3−ε) magnetic reflection by measuring diffraction profiles along the receprocal c^* axis at each temperature. The results are shown in Fig. 5(a). Two sets of profiles are presented for the respective temperature data and correspond to the reflection from left- and right-handed spiral domains. The (0 0 3−ε) magnetic reflection develops as temperature is decreased below T_N. The value of ε gradually decreases with decreasing temperature and is essentially consistent with that reported in a former neutron diffraction study.[15] Before every mapping measurement, we oriented the crystal to diffract on the (0 0 3−ε) magnetic reflection at each temperature.

Figures 5(c)–5(e) show the observed intensity maps, i.e., spin chiral domains, at 273, 248, and 198 K, respectively. Figure 5(b) displays a photograph of the crystal surface measured for this experiment. The measurements were done during the cooling process after the sample was heated to 330 K ($>T_N$). Each figure has a different scale of intensity. Although the contrast gradually becomes intense with decreasing temperature, the domain patterns at these three temperatures are qualitatively similar to one another. However, once the crystal is heated above T_N, the domain pattern changes. The intensity map shown in Fig. 5(f) was taken for the same area at 47 K, but the crystal was again heated to 330 K($>T_N$) before the measurement. The domain structure shown in Fig. 5(f) is different from those shown in Figs. 5(c)–5(e). (In the absence of magnetic fields, there is no phase transition below T_N in the hexaferrite.[15]) These results suggest that the domain structure is robust with respect to the variation of temperature and time once the spin-chiral domains are formed but is not reproducible once the crystal is heated above T_N.

IV. CONCLUSIONS

We investigated spatial maps of spin-chiral domains in helimagnetic $Ba_{0.5}Sr_{1.5}Zn_2Fe_{12}O_{22}$ by means of a scanning resonant x-ray microdiffraction technique using a circularly polarized and highly focused x-ray beam. This technique provides the necessary resolution and contrast to resolve self-organizing spin-chiral domains on clean surfaces of helimagnets. We observed that domains are on a submillimeter-length scale and robust with respect to the variation of time and temperature once they form. This suggests that the spin-chiral domains can be used for a recording medium, because the two chiral states can be switched by electric and/or magnetic fields through magnetoelectric couplings.

ACKNOWLEDGMENTS

This work was supported by Grants-in-Aid for Scientific Research (Grant Nos. 21244049, 20674005, 20001004, and 19052001) and the Global COE Program (Program No. G10), Ministry of Education, Culture, Sports, Science, and Technology, Japan. Experiments were performed at beamline 17SU in SPring-8 with approval of RIKEN (Proposal No. 20100020).

*kimura@mp.es.osaka-u.ac.jp

[1] A. Yoshimori, J. Phys. Soc. Jpn. **14**, 807 (1959).
[2] S.-W. Cheong and M. Mostovoy, Nature Mater. **6**, 13 (2007).
[3] N. Nagaosa, J. Sirova, S. Onoda, A. H. MacDonald, and N. P. Ong, Rev. Mod. Phys. **82**, 1539 (2010).
[4] O. Nakanishi, A. Yanase, A. Hasegawa, and M. Kataoka, Solid. State Commun. **35**, 995 (1980).
[5] P. Bak and M. H. Jensen, J. Phys. C **13**, L881 (1980).
[6] G. Shirane, R. Cowley, C. Majkrzak, J. B. Sokoloff, B. Pagonis, C. H. Perry, and Y. Ishikawa, Phys. Rev. B **28**, 6251 (1983).
[7] K. Siratori, J. Akimitsu, E. Kita, and M. Nishi, J. Phys. Soc. Jpn. **48**, 1111 (1980).
[8] S. B. Palmer, J. Baruchel, A. Drillat, C. Patterson, and D. Fort, J. Magn. Magn. Mater. **54–57**, 1626 (1986).
[9] J. Baruchel, Physica B **192**, 79 (1993).
[10] J. C. Lang, D. R. Lee, D. Haskel, and G. Srajer, J. Appl. Phys. **95**, 6537 (2004).
[11] P. G. Evans and E. D. Isaacs, J. Phys. D: Appl. Phys. **39**, R245 (2006).
[12] E. Schierle, V. Soltwisch, D. Schmitz, R. Reyerherm, A. Maljuk, F. Yokaichiya, D. N. Argyriou, and E. Weschke, Phys. Rev. Lett. **105**, 167207 (2010).
[13] F. Fabrizi, H. C. Walker, L. Paolasini, F. de Bergevin, T. Fennell, N. Rogado, R. J. Cava, T. Wolf, M. Kenzelmann, and D. F. McMorrow, Phys. Rev. B **82**, 024434 (2010).
[14] T. Kimura, G. Lawes, and A. P. Ramirez, Phys. Rev. Lett. **94**, 137201 (2005).
[15] N. Momozawa and Y. Yamaguchi, J. Phys. Soc. Jpn. **62**, 1292 (1993).
[16] A. M. Mulders, S. M. Lawrence, A. J. Princep, U. Staub, Y. Bodenthin, M. García-Fernández, M. Garganourakis, J. Hester, R. Macquart, and C. D. Ling, Phys. Rev. B **81**, 092405 (2010).
[17] N. Momozawa, M. Mita, and H. Takei, J. Cryst. Growth **83**, 403 (1987).
[18] T. Takeuchi, A. Chainani, Y. Takata, Y. Tanaka, M. Oura, M. Tsubota, Y. Senba, H. Ohashi, T. Mochiku, K. Hirata, and S. Shin, Rev. Sci. Instrum. **80**, 023905 (2009).
[19] L. D. Landau and E. M. Lifshitz, *Quantum Electrodynamics,* 2nd ed., Vol. 4 (Pergamon, Oxford, 1982).
[20] H. Ohashi, Y. Senba, H. Kishimoto, T. Miura, E. Ishiguro, T. Takeuchi, M. Oura, K. Shirasawa, T. Tanaka, M. Takeuchi, K. Takeshita, S. Goto, S. Takahashi, H. Aoyagi, M. Sano, Y. Furukawa, T. Ohata, T. Matsushita, Y. Ishizawa, S. Taniguchi, Y. Asano, Y. Harada, T. Tokushima, K. Horiba, H. Kitamura, T. Ishikawa, and S. Shin, AIP Conf. Proc. **879**, 523 (2007).